

# Tidal deformation of dynamical horizons in binary black hole mergers

Vaishak Prasad,<sup>1</sup> Anshu Gupta,<sup>1</sup> Sukanta Bose,<sup>1,2</sup> and Badri Krishnan<sup>3,4,5</sup>

<sup>1</sup>*Inter-University Centre for Astronomy and Astrophysics, Post Bag 4, Ganeshkhind, Pune 411 007, India*  
<sup>2</sup>*Department of Physics and Astronomy, Washington State University, 1245 Webster, Pullman, WA 99164-2814, U.S.A*

<sup>3</sup>*Max-Planck-Institut für Gravitationsphysik (Albert Einstein Institute), Callinstr. 38, 30167 Hannover, Germany*

<sup>4</sup>*Leibniz Universität Hannover, Welfengarten 1-A, D-30167 Hannover, Germany*

<sup>5</sup>*Institute for Mathematics, Astrophysics and Particle Physics, Radboud University, Heyendaalseweg 135, 6525 AJ Nijmegen, The Netherlands*

(Dated: June 24, 2022)

An important physical phenomenon that manifests itself during the inspiral of two orbiting compact objects is the tidal deformation of each under the gravitational influence of its companion. In the case of binary neutron star mergers, this tidal deformation and the associated Love number have been used to probe properties of dense matter and the nuclear equation of state. Non-spinning black holes on the other hand have a vanishing (field) tidal Love number in General Relativity. This pertains to the deformation of the asymptotic gravitational field. In certain cases, especially in the late stages of the inspiral phase when the black holes get close to each other, the *source* multipole moments might be more relevant in probing their properties and the No-Hair theorem; contrastingly, these Love numbers do *not* vanish. In this paper, we track the source multipole moments in simulations of several binary black hole mergers and calculate these Love numbers. We present evidence that, at least for modest mass ratios, the behavior of the source multipole moments is universal. [This manuscript has been assigned the LIGO Preprint number [LIGO-P2100109](#).]

## I. INTRODUCTION

The general treatment of the tidal deformation of compact objects has been perturbative. In such a treatment, an external tidal field is taken to induce a deformation of the compact object. The contribution of that field can be distinguished from the field of the object itself, e.g., when the former is treated perturbatively. Every  $l^{\text{th}}$  multipolar order of the external tidal field induces an  $l^{\text{th}}$  multipolar moment in the configuration of the compact object, and the constant of proportionality relating these is called a Love number.

A sizeable literature exists on applications of tidal deformation and Love numbers [1–3], especially, in how they encode information about neutron star equation of state [4] in gravitational-wave signals [5–7]. On the other hand, tidal deformations of black holes and the associated Love numbers are discussed in, e.g., Refs. [8–10] for the non-spinning case and Refs. [11–13] for the spinning case.

Since black holes are solutions to vacuum field equations, the usual definition of the multipolar configuration of the system involving an integral of the mass density of the system is irrelevant here. Instead, one has to address how the external tidal field induces a change in the geometry of the horizon. The information of the geometry of the horizon is encoded in the source/geometric multipole moments as opposed to the field multipole moments. One may expect a similar relation between the geometric multipoles and the  $l^{\text{th}}$  order multipolar external tidal field.

Past treatments of tidal deformability typically start either with the assumption that there exists a source distribution that is deformed due to an external tidal field [14]

or involve the application of black hole perturbation theory [8–13].

A limit of the compactness is then taken to deduce the corresponding Love numbers for black holes.

The problem with the “limiting compactness” approach is that black holes do not have a source distribution. Furthermore, in a true sense, the horizons of black holes cease to be null hypersurfaces in a dynamical tidal environment and are no longer isolated. Hence, it is desirable to employ an alternative treatment with a differently defined set of quantities that characterize the tidal deformability of black holes. In this sense, the dynamical horizon formalism is an ideally suited framework to treat the problem of the tidal deformation of black holes. In that formalism, for black holes in a vacuum, a set of numbers – called the geometric/source multipole moments – fully characterize the horizon geometry. In a tidal environment, these numbers can change, e.g., owing to an alteration in the horizon geometry in response to the external tidal field.

In this work, we address this question in a binary black hole merger scenario. We describe and use a convenient definition of tidal deformability suited to a binary black hole system and compute them numerically using full numerical relativity simulations of binary black hole mergers of non-spinning black holes. We use the framework of quasi-local horizons for our analysis; see e.g. [15, 16] for reviews. We use the source multipole moments to address this question. In particular, we use the mass and spin multipole moments to characterize the deformation in the horizon geometry and define a set of dimensionless tidal coefficients. We then calculate the leading order tidal coefficients that characterize the deformation of a black hole in the tidal environment of its companion in

a binary black hole merger scenario using full numerical relativity.

The plan for the rest of the paper is as follows. Sec. II briefly reviews basic concepts and equations for dynamical horizons and describes the definition of the geometric/source multipole moments of horizons. The details of Numerical simulations are given in Sec. III. In Sec. IV we compute the tidal coefficients and describe the fitting procedure. The results are summarised in Sec. V followed by Sec. VI with discussion and conclusions. Appendix A contains comparison of distance measures among centroid distance and various orders of post-Newtonian approximations.

All the equations and quantities are expressed in geometric units, where  $G = c = 1$ . The masses of the primary and secondary black holes in the initial data are  $M_1$  and  $M_2$ , and their mass ratio is defined to be  $q \equiv M_2/M_1$ , which is always  $\leq 1$ . Additionally, the total mass of the black holes in the initial data, denoted by  $M = M_1 + M_2$  is set to one. In a few places where tracking the dependence on  $M$  is important, we show it explicitly.

## II. PRELIMINARIES

Our calculation of the tidal deformations of black holes is based on the formalism of quasi-local horizons [15–21]. A detailed description of this formalism is beyond the scope of this article and we shall restrict ourselves to a brief overview of the most relevant concept, namely, that of black hole source multipole moments.

The starting point is the notion of a marginally trapped surface, first introduced by Penrose in the context of the black hole singularity theorems [22]. More specifically we need here the notion of marginally outer trapped surfaces (MOTS), which are closed space-like 2-dimensional surfaces of spherical topology, such that their outgoing null-normals  $\ell^a$  have vanishing expansion  $\Theta_{(\ell)}$ . Thus, if  $\mathcal{S}$  is a MOTS,  $q_{ab}$  the Riemannian metric on  $\mathcal{S}$ , and  $\ell^a$  an outward-pointing null-normal to  $\mathcal{S}$ , then a MOTS has

$$\Theta_{(\ell)} := q^{ab} \nabla_a \ell_b = 0. \quad (1)$$

Under time evolution, a MOTS  $\mathcal{S}$  traces out a 3-dimensional world tube sometimes referred to as a dynamical horizon [23, 24], or a marginally trapped tube [25, 26]. We shall not delve here into properties of this time evolution. We shall instead just consider various properties of  $\mathcal{S}$  as functions of time. It turns out that the time evolution of MOTS is generally found to be smooth, which means that we end up with smooth functions of time. When two black holes collide, the process by how two distinct dynamical horizons merge to yield a single final dynamical horizon turns out to have interesting topological and dynamical properties [27–30]. Again, this is beyond the scope of this paper. Here, we shall

only consider the two dynamical horizons corresponding to the two individual black holes before they merge.

For each of the two dynamical horizons, we shall calculate the geometric/source multipole moments. These were first introduced in [31] for isolated horizons, and extended and used in [32] for dynamical horizons. These multipole moments have found applications, for example, in predictions of the anti-kick in binary black hole mergers [33] and for studying tidal deformations of black holes [34–36].

For defining these multipole moments, let  $\mathcal{S}$  be a MOTS on a Cauchy surface  $\Sigma$ . Let  $K_{ab}$  be the extrinsic curvature of  $\Sigma$  embedded in spacetime,  $r^a$  the unit space-like normal to  $\mathcal{S}$  and tangent to  $\Sigma$ . Let the areal radius of  $\mathcal{S}$  be denoted by  $R_{\mathcal{S}}$ , its mass by  $M_{\mathcal{S}}$  and angular momentum by  $J_{\mathcal{S}}$ . Furthermore, let  $\mathcal{S}$  be axisymmetric and let  $\varphi^a$  be the axial symmetry vector field on  $\mathcal{S}$ . The symmetry vector  $\varphi^a$  can be used to construct a preferred coordinate system  $(\theta, \varphi)$  on  $\mathcal{S}$  analogous to the usual spherical coordinates on a sphere; let  $\zeta = \cos \theta$ . We can then use spherical harmonics in this preferred coordinate system to construct multipole moments. As expected we have two sets of moments  $M_n, J_n$  such that  $M_0$  is the mass  $M_{\mathcal{S}}$  and  $J_1$  is the angular momentum  $J_{\mathcal{S}}$ . The expressions for the multipole moments are the following

$$M_n = \frac{M_{\mathcal{S}} R_{\mathcal{S}}^n}{8\pi} \oint_S \tilde{\mathcal{R}} P_n(\zeta) d^2S, \quad (2)$$

and

$$J_n = \frac{R_{\mathcal{S}}^{n-1}}{8\pi} \oint_S P'_n(\zeta) K_{ab} \varphi^a r^b d^2S, \quad (3)$$

where  $P_n(\zeta)$  is the  $n^{\text{th}}$  Legendre polynomial and  $P'_n(\zeta)$  its derivative.

In a binary black hole merger scenario, the individual horizons of the black holes are dynamical and many of the above assumptions do not hold. For example, the  $\Psi_2$  of the two black holes are not time-independent, and neither are their areas, curvature, and other geometric quantities on  $\mathcal{S}_t$ . However, following [32], we shall continue to interpret the surface density and current in the same way so that the multipole moments share the same definitions as above. These multipole moments are gauge independent in the same sense as a dynamical horizon is gauge independent, i.e., they exist as geometric objects in spacetime independent of the spacetime foliation used to locate them. A different choice of spacetime slicing will give a different dynamical horizon, but for any given dynamical horizon, the multipole moments are gauge independent.

We attempt to understand the tidal deformation of the horizons using the dynamical horizon formalism. The horizon geometry is characterized by the mass and spin multipole moments of the dynamical horizon. The presence of the companion induces a change in the horizon geometry of the black holes. Notably, the 2-Ricci scalar

$(\tilde{\mathcal{R}})$  of the two-dimensional slices of the dynamical horizons change from their equilibrium configuration when the horizons are isolated. During the inspiral phase, the two black holes influence each other and mutually change the other's horizon geometry. As they inspiral toward each other in the tidal environment of their companion, both the dynamical horizons suffer mutual changes in their intrinsic geometries. This is captured by the change in the mass and spin multipole moments of the dynamical horizons through Eqs. (2), (3). In this work, since we deal with non-spinning black holes, we attempt to understand the tidal deformability of black holes using mass multipole moments.

The description given in the previous paragraph can be understood better through Fig. 1, where the Ricci scalars of a two-dimensional slice of the dynamical horizons of the two black holes in a binary system are plotted. The plot is such that the portions of the horizons of the black holes facing each other at a particular time step during the inspiral phase of the merger are facing towards the reader. As the two black holes inspiral towards each other, the Ricci scalar distribution pattern continues to face each other at all points on the orbit although the individual values change (this can be seen in the movie which can be accessed through the link provided in the caption). This effect is due to the presence of their companions. More details about the computations and numerical setup will be found in subsequent sections. The quadrupolar mode structure and the quantitative details of the evolution of the 2-dimensional Ricci scalar distribution of the leaves of each of the dynamical horizons are captured in the time-series of  $l = 2$  mass-multipole moments computed at each time step in the simulation. In this work, using the evolution of this  $l = 2$  mass-multipole moment of the dynamical horizons of both the black holes, we define and attempt to compute dimensionless tidal coefficients/Love numbers that universally characterize the tidal deformability of black holes.

We now describe the procedure to estimate the coefficients that characterize the  $l = 2$  mass multipolar deformation of the horizon geometry using full numerical relativity simulations of BBH mergers.

Turning now to our object of interest, namely a binary black hole system in the inspiral/pre-merger phase. Imagine starting with two Kerr black holes far apart, with the source mass and spin multipoles  $(\mathcal{M}_n, \mathcal{J}_n)$  defined above exactly as for a Kerr black hole. As the black holes spiral in and approach each other, these multipole moments will vary under the influence of the gravitational field of the other. Let the variation in  $\mathcal{M}_n$  and  $\mathcal{J}_n$  be respectively  $\delta\mathcal{M}_n$  and  $\delta\mathcal{J}_n$  (these will be functions of time). In general, this deformation of the multipole moments will depend on the mass and spin of the companion, the separation  $d$  between the black holes, and also possibly on the relative velocity. We restrict ourselves to the simpler situation of non-spinning black holes, and also ignore the relative velocity. Furthermore, we require that in the limit  $d \rightarrow \infty$ ,  $\mathcal{M}_n$  and  $\mathcal{J}_n$  should vanish.

From dimensional arguments, we are then naturally led to an expansion of the multipole moments of the black hole whose deformation is being studied  $M_{td}$  due to the tidal field of its companion  $M_{tf}$  of the form:

$$\frac{\delta\mathcal{M}_n}{M_{td}^{n+1}} = \sum_{i,j=1}^{\infty} \alpha_{ij}^{(n)} \frac{M_{td}^i M_{tf}^j}{d^{i+j}}. \quad (4)$$

Such an expansion has been previously used to understand the tidal deformations of black holes in the Bowen-York initial data set [34]. Along the same lines,

the following observations can be made on the above expansion. Firstly, the expansion must start at  $i = j = 1$  since when we take the limit of either of the masses tending to zero, the LHS must vanish. Also, there will be no positive exponents on the distance measure  $d$ ; i.e.,  $\delta\mathcal{M}/\mathcal{J} \propto d^{\nu > 0}$  as the perturbation should vanish in the limit  $d \rightarrow 0$ . The coefficients  $\alpha_{ij}^{(n)}, \beta_{ij}^{(n)}$  are dimensionless coefficients independent of the system as they have been scaled out by appropriate factors. These coefficients are therefore the same for all black holes and are thus universal. They should characterize the tidal deformability of the black holes.

### III. NUMERICAL SIMULATIONS OF BINARY BLACK HOLE MERGERS

We ran numerical simulations of orbital mergers for a set of non-spinning binary black holes with varying mass ratios. The systems are evolved numerically using puncture data [37] describing two black holes in quasi-circular orbits, with typical initial separations of  $10-11M$ . These simulations cover the dynamical behavior starting at 5-6 orbits before the merger and going up to the merger phase. The gravitational waveform is extracted [38] at various distances between  $100M$  to  $500M$  from the merger location.

Since this work is focused on the study of individual horizon geometry of the black holes in the inspiral phase, we track the individual horizons up to merger and compute quasi-local quantities [32, 39] using the isolated and dynamical horizon formalism [15].

Simulations are performed using publicly available code Einstein Toolkit [40, 41]. The initial data is generated based on the puncture approach [42], which has been evolved through BSSNOK formulation [43–45] using the  $1 + \log$  slicing and  $\Gamma$ -driver shift conditions.

The computational grid set-up is based on the multi-patch approach using Llama [46] and Carpet modules, which enable the mapping and coordinate transformation of multigrid set up from curvilinear coordinates to Cartesian along with adaptive mesh refinement (AMR). It helps to optimally evolve spacetime for a long time in a larger computational domain and to extract gravitational waves at faraway regions as compared to the Cartesian grid. Individual horizons and common horizons on the numerical grid are found via the method described in

[47, 48]. We compute the quasi-local quantities on the horizon on an angular grid of size (37, 76) along the longitudinal and latitudinal directions, respectively.

We consider non-spinning binary black hole systems with varying mass-ratio  $q = M_2/M_1$ , where  $M_{1,2}$  are the masses of the primary and secondary objects. The larger blackhole with mass  $M_1$  will be denoted by BH1 and the smaller one with mass  $M_2$  by BH2. We will be studying the tidal deformation of both the black holes BH1 and BH2 due to their companion.

We use GW150914 parameter file available from [49], as the template for our simulations. For each case, as input parameters, we provide initial separation between the two punctures  $D$ , mass ratio  $q$  and radial and azimuthal linear momentum  $p_r, p_\phi$  respectively, while keeping the total horizon mass  $M = M_1 + M_2$  of the system to be 1.0, in units of  $c = G = M = 1$ . Parameters are listed in Table I. We compute the corresponding initial locations, the  $x, y, z$  components of linear momentum for both black holes, and grid refinement levels, etc., before generating the initial data and evolving it. We chose non-spinning cases ranging between  $q = 1.0$  to 0.4, based on the initial parameters listed in [50, 51]. Our simulations match very well with the catalog simulations [52], having merger time discrepancies of less than a few percent.

Note that since the horizon masses of the two black holes evolve during the inspiral, they deviate from the physical masses  $M_{1,2}$  in the initial data. However, the fractional deviation turns out to be sub-percent in the analysis domain (i.e.,  $\lesssim 0.1\%$ ). Therefore, for this work these masses can be safely assumed to remain constant throughout the evolution.

#### IV. COMPUTING THE TIDAL COEFFICIENTS

We now describe a method to compute the leading and sub-leading order tidal coefficients appearing in the expressions for the expansion of the perturbed multipole moments numerically using the aforementioned simulations of BBH mergers.

To distinguish between the black hole that is tidally deformed and the black hole that sources the tidal field we use  $M_{td}$  for the former and  $M_{tf}$  for the latter. Thus,  $M_{td}$  can be  $M_1$  and  $M_{tf}$  can be  $M_2$  or vice-versa depending on whether the tidal deformation of  $M_1$  is being studied or that of  $M_2$ . We denote an alternate-mass ratio defined using  $M_{td}$  and  $M_{tf}$  by  $\gamma$ :

$$\gamma = \frac{M_{tf}}{M_{td}} \quad (5)$$

As opposed to the mass ratio defined earlier in Table I,  $\gamma$  takes values in the range [0.4, 2.25].

#### A. Identification of the leading order term

We begin by noting that Eq. (4) is a power-series in the distance of separation of the two orbiting black holes. We postulate that there would be no term at order less than  $1/d^3$  (i.e., no term involving a lower exponent on  $1/d$ , such as  $1/d^2$  or  $1/d$ ) since the Newtonian tidal force enters as  $\propto 1/d^3$ . Therefore, the leading term is  $\mathcal{O}(1/d^3)$ . The sub-leading order term is  $\mathcal{O}(1/d^4)$  and is responsible for post-Newtonian tidal influences. Henceforth, we will use *third-order* and *fourth-order* to refer to the exponent on the distance, with the third-order term being the leading and the fourth-order being the sub-leading term.

The expression for the perturbative expansion for  $l = 2$  mass multipole moment at the leading (Model A), and leading and sub-leading (Model B) order perturbations due to  $M_{tf}$  are, respectively,

$$\text{Model A} : \frac{\mathcal{M}_2}{M_{td}^3} = \frac{a_3^{(2)}}{d^3} + \text{const.} \quad (6)$$

and

$$\text{Model B} : \frac{\mathcal{M}_2}{M_{td}^3} = \frac{a_3^{(2)}}{d^3} + \frac{a_4^{(2)}}{d^4} + \text{const.} \quad (7)$$

Here, the tidal coefficients are related to  $a_3^{(2)}$  and  $a_4^{(2)}$  through:

$$a_3^{(2)} = M_{td} M_{tf}^2 \alpha_{12}^{(2)} + M_{td}^2 M_{tf} \alpha_{21}^{(2)}, \quad (8)$$

$$a_4^{(2)} = \alpha_{13}^{(2)} M_{td} M_{tf}^3 + \alpha_{22}^{(2)} M_{td}^2 M_{tf}^2 + \alpha_{31}^{(2)} M_{td}^3 M_{tf}. \quad (9)$$

Note, that in the case of an isolated non-spinning black hole, the horizon geometry is spherically symmetric, therefore, the  $l = 2$  mass multipole moment is zero, resulting in  $\delta\mathcal{M}_2 = \mathcal{M}_2$ . However, in the above model, we include an overall constant in the fits to allow for any systematic errors in the numerical computation of the multipole moment and to take into account the fact that the initial data is described by punctures and not real black holes. We use the distance measure which is computed by the simple Euclidean separation between the geometric centroids of the two black holes at every time step in the simulation. This agrees well with the physical distance measures between the black holes. More details can be found in Appendix A.

We will now detail the procedure for computing the tidal coefficients  $\alpha_{12}^{(2)}, \alpha_{21}^{(2)}, \alpha_{13}^{(2)}, \alpha_{22}^{(2)}$  and  $\alpha_{31}^{(2)}$  using these models. Thereafter, we compare the fits obtained. The superscript (2) is used to denote the fact that we are analyzing  $l = 2$  mass multipole moment; since this paper deals exclusively with  $l = 2$  mass multipolar deformations, it will be dropped henceforth. Resolving higher  $l$  multipole moments would require a sufficiently fine grid on the horizon. Due to computational limitations, we restrict our analysis to  $l = 2$  multipolar deformations in this work.

Non-spinning BBH Simulations					
Mass ratio	$d$	$M_1$	$M_2$	$p_r$	$p_t$
1.0	11.0	0.5	0.5	-7.220e-04	0.09019
0.85	12.0	0.54051	0.4595	-5.290e-04	0.08448
0.75	11.0	0.5714	0.4286	-6.860e-04	0.08828
0.6667	11.75	0.6	0.4000	-5.290e-04	0.08281
0.50	11.0	0.6667	0.3333	-5.720e-04	0.0802
0.40	11.25	0.7143	0.2857	-4.500e-04	0.07262

TABLE I: Initial parameters for non-spinning binary black holes with quasi-circular orbits. Here,  $q = M_2/M_1$  is the mass-ratio,  $d$  is the initial separation between the two holes,  $p_r$  and  $p_t$  are the radial and tangential (to the orbit) momenta in the initial data, respectively.

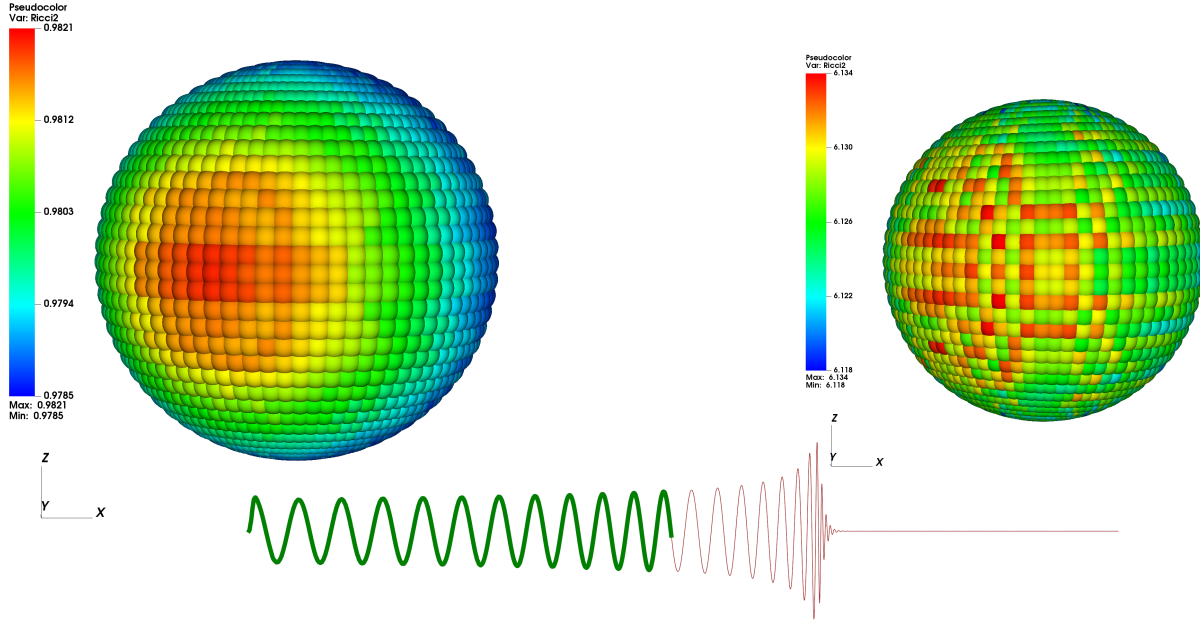


FIG. 1: The change in the mass multipole moments of the black holes Eq. (2) can also be directly visualized in terms of the 2-Ricci scalar  $\bar{R}$  of the two-dimensional slices of the dynamical horizon. Here the 2-Ricci scalars of the time slices of the two dynamical horizons are visualized for the  $q = 0.4$  system when the black holes are at a separation of  $d \approx 7.5M$  (about 66% of the initial separation). This is approximately 5 orbits after the start of the simulation, as shown by the thick green line in the waveform plot below the figure. The total number of orbits before the merger is around 9 and the corresponding complete waveform cycles in the simulation are shown by the thin red line. The more massive black hole 1 is on the left. The values of the Ricci scalar are shown on the color bars to the left of each black hole. The lengths are not to scale. In the actual simulation, the  $z$ -axes of the two black holes are aligned as shown here, and one black hole is behind the other, i.e., the Ricci scalar patterns are aligned along the line joining the two black holes. A movie for  $q = 0.6$  can be viewed [here](#) [53]. This movie shows that the deformation of the horizon geometry is mutual for both the horizons and the Ricci scalar distribution patterns face each other at all points on the orbit. 3D visualizations were performed using *VisIt* [54]

## B. The Fitting procedure

To estimate the tidal coefficients we follow a two-step fitting procedure:

1. Fit of multipole moment data to distance, sepa-

rately to each of the simulations and black holes, and estimating the coefficients  $a_3$  and  $a_4$  using the model Eq. (7).

2. The re-fitting of all values of the best-fit parameters from the above step to the masses  $M_{td}$  and  $M_{tf}$ , in

a combined manner, to the models in Eqs. (8) and (9) to obtain the tidal coefficients  $\alpha_{ij}$ .

We carry out linear regression of the numerical data in two steps to fit the numerical data to the models. We minimize a least-squares objective function in the process. We directly compute a least-squares objective function on a grid in the parameter space and locate the minimum. Since this method is computationally expensive, we follow the two step procedure mentioned above.

For carrying out the regression, we relate the models and the data in a matrix form as

$$Y = XA, \quad (10)$$

where  $Y$  is a matrix of dimensions  $(K, 1)$  of the left-hand side of the respective model,  $X$  is the matrix of data points of dimensions  $(K, L)$  and  $A$  the matrix of the parameters of dimensions  $(L, 1)$ . For instance, in the fitting procedure of step one,  $K$  is equal to the number of data points in the time-series data of the multipole moment/distance and  $L$  is the number of parameters in the model (which is 3 for Model B).

We use the following least-squares objective function in the minimization procedure (the summation convention is assumed on repeating indices):

$$\mathcal{L}(A) = \sum_i (Y_i - X_{ij}A_j)^2, \quad (11)$$

Here  $X_{ij}A_j$  is the prediction from the respective linear models. The linearization of the above models in Eqs. (6), (7), (8), and (9) is done by assuming the fitting parameters as coefficients of a linear variable. To exemplify this, let us consider the two steps of the fitting procedure for Model B. In step one, the linearized model corresponding to Eq. (7) would be written as:

$$\frac{\mathcal{M}_2}{M_{td}^3} = a_3x_3 + a_4x_4 + \text{const.}, \quad (12)$$

where  $x_3 = 1/d^3$  and  $x_4 = 1/d^4$  are the linear fitting variables. For re-fitting, Eqs. (8) and (9) would be used. The re-fitting model corresponding to Eq. (9) would be written as:

$$a_4 = \alpha_{13}\mu_{13} + \alpha_{22}\mu_{22} + \alpha_{31}\mu_{31}, \quad (13)$$

where  $\mu_{13} = M_{td}M_{tf}^3$ , and so on.

### 1. Error estimation

The best-fit parameter values (denoted by  $\hat{A}$ ) are those that minimize the least-squares objective function Eq. (11) for the respective models. We compute the errors on the best-fit parameter values from the diagonal components of the variance-covariance matrix  $\mathcal{C}$  of the data, and the fit residue  $\sigma_{fit}$ :

$$\mathcal{C} = X^T X \quad (14)$$

and

$$\sigma_{fit} = \sqrt{\mathcal{L}(\hat{A})} \quad (15)$$

as

$$\sigma(\hat{A}) = \sigma_{fit} \times \text{Diag}(\mathcal{C}). \quad (16)$$

Here, the matrix of best-fit parameters is denoted by  $\hat{A}$  and their standard error of estimates by  $\sigma(\hat{A})$ . We will refer to the individual elements of these matrices by  $\hat{A}_j$  and  $\sigma_j$  respectively. Since these parameters can correspond to the fitting procedure of either step one or step two, we will explicitly mention which step we are referring to during their usage.

## V. RESULTS

We obtain the best-fit parameters for the two models Eq. (6) and Eq. (7) using the two-step procedure mentioned in the preceding section and tabulate the results in Table II. In this table, the final results of the step two of the fitting procedure (i.e. re-fits to the models in Eqs. (8) and (9)) are denoted in the format  $\hat{A}_j \pm \sigma_j$ : the best-fit parameter value and the respective standard error.

In Fig. 2, we show the fit of the  $l = 2$  mass multipole moment to the two models Eq. (6) (Model A) and Eq. (7) (Model B) for  $q = 0.4$  simulation data. In these plots, we show the data points and the best fitting model i.e. the values of the  $l = 2$  multipole moment  $\mathcal{M}_2$  predicted by the models in Eqs. (6) and (7) for the best fit parameter values  $\hat{A}$ . In the top panel, we plot the multipole moment data *vs* the distance of separation for the more massive black hole (left) and the less massive black hole (right). In the bottom panel, we plot the same in log scale on both axes. As can be seen, Model B, consisting of both  $1/d^3$  and  $1/d^4$  terms, fits the data better in comparison to Model A (which has only the  $1/d^3$  term).

In Figs. 3 and 4, we show the results of step two of the fitting procedure (re-fitting results) of the parameters  $a_3$  and  $a_4$  of Model B appearing in Eq. (8) and Eq. (9), respectively, which were obtained from step one of the fit for the set of binary black hole configurations as listed in Table I. In these plots, we show the data points and the best fitting model i.e. the values of  $a_3$  and  $a_4$  predicted by the models in Eqs. (8) and (9) for the best fit parameter values  $\hat{A}$ .

Some comments are in order regarding these fits. Firstly, we can see that the leading order model (Model A) fits the data for the heavier black hole (left panel of Fig. 2) quite well especially in the early inspiral phase, i.e., at large distances of separation between the black holes. Since the system spends more time in the early inspiral phase (at large distances of separation), there are more points at large  $d$  to which the model fits well. However, this model fails to explain the data as the black holes close in. This is expected because the

Tidal coefficients					
Model	$\alpha_{12}$	$\alpha_{21}$	$\alpha_{13}$	$\alpha_{22}$	$\alpha_{31}$
third-order model	$-0.15 \pm 0.21$	$-3.43 \pm 0.21$	NA	NA	NA
Third and fourth-order model	$-0.89 \pm 0.21$	$-5.45 \pm 0.21$	$1.79 \pm 1.72$	$5.3 \pm 3.65$	$4.68 \pm 1.72$

TABLE II: Tidal coefficient values estimated from a re-fit of the fit coefficients  $a_3$  and  $a_3, a_4$  in Eq. (6) and Eq. (7), respectively. The error bars begin differing at the third decimal place.

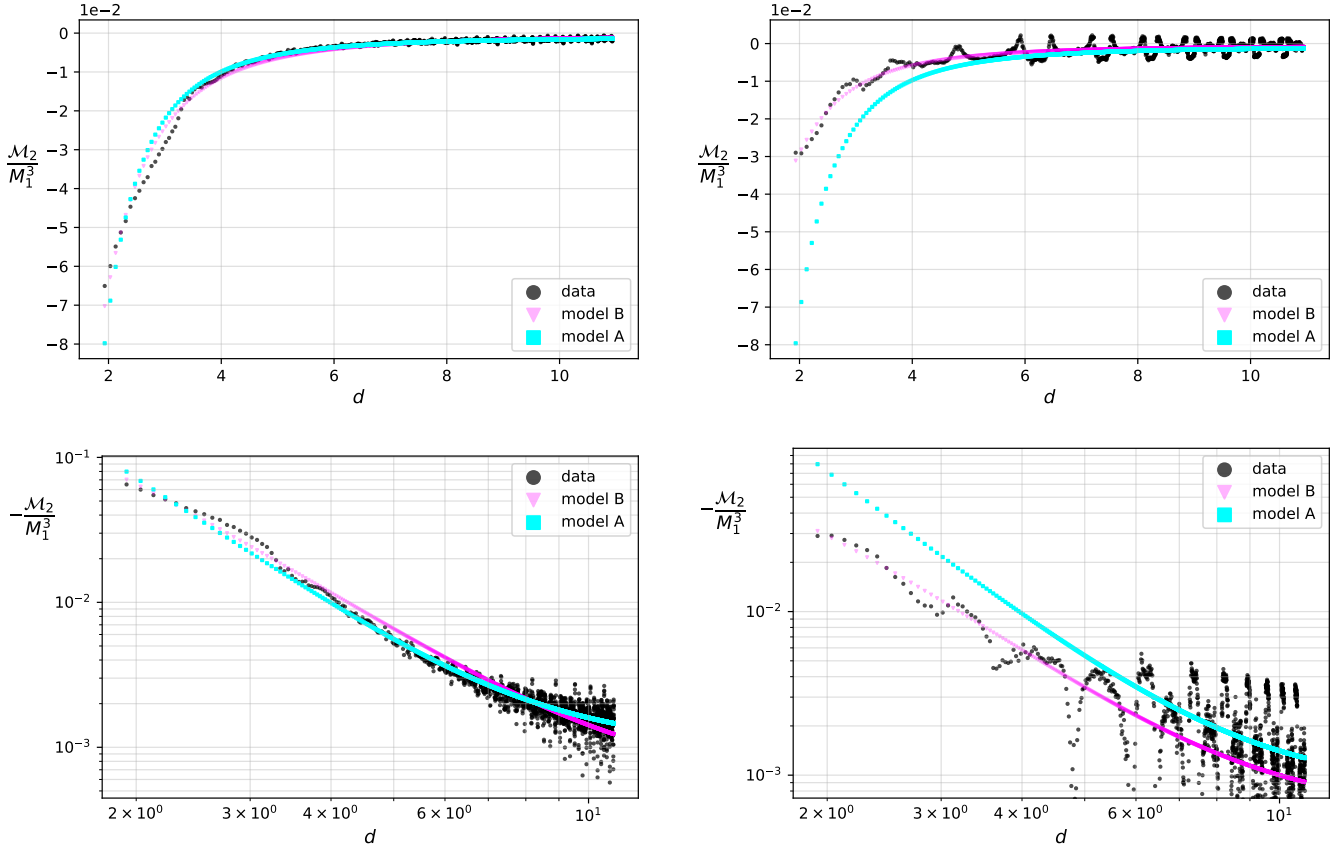


FIG. 2: The fit of the  $l = 2$  mass multipole moment of BH1 (left) and BH2 (right) for the simulation  $q = 0.4$ . **Top:** The multipole moment data is plotted against the distance  $d$ .

**Bottom:** The multipole moment data and the distance  $d$  are plotted in a logarithmic scale. Note that the variable on the  $y$ -axis contains the negative of the multipole moment in the bottom figure.

In these two figures, the model where only the leading (third) order term is included (namely, Model A of Eq. (6)) is shown in cyan (squares) whereas the model where the leading and sub-leading order terms have been included (namely, Model B of Eq. (7)) is shown in magenta (triangles). The data is in black (dots).

sub-leading term in Eq. (7) is expected to become increasingly important at low separation distances  $d$ . This is where we expect Model B to be more accurate.

Secondly, the quality of fit of the leading order model to the data: The fit of Model A is visibly worse for the smaller black hole (right panels of Fig. 2). From a perturbative point of view, we can intuitively explain this as follows. The change in the geometry of the smaller black hole due to the presence of the larger black hole is more than the change in geometry, quantified by the multipole moments, of the larger black hole due to the smaller one,

as the larger black hole is more massive leading to more variations in its multipole moment.

The sub-leading (fourth) order term contains higher powers of the perturbing black hole's mass  $M_{tf}$  than at the leading (third) order ( $M_{tf}^3$  as opposed to  $M_{tf}^2$  in Eq. (8) and (9)). Therefore, the effect of the fourth-order term will be easily visible in the multipole moment of the smaller black hole  $M_2$  (see right panels in Fig. 2) and the fit between data and Model A is visibly worse in the plots for the smaller black hole.

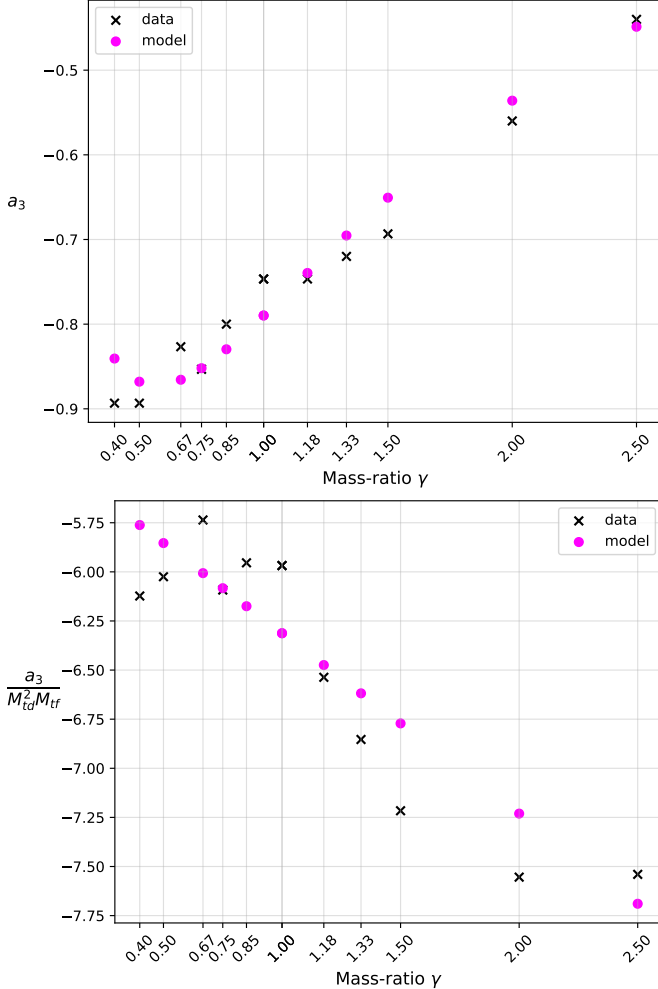


FIG. 3: The re-fit of the coefficient  $a_3$  to obtain the tidal coefficients in Eq. (8) (Model B). **Top:**  $a_3$  vs  $\gamma$ . **Bottom:**  $a_3/(M_{td}^2 M_{tf})$  vs  $\gamma$ , i.e., the  $y$  axis of the bottom figure is obtained by scaling that in the top figure by the mass combination  $M_{td}^2 M_{tf}$ . The data points are individual best fit parameters of Model B in Eq. (9) for both black holes in each simulation. The data points for the fit are in **black (crosses)** and the best fit model values are in **magenta (dots)**.

Thirdly, the fourth-order term has the opposite sign to that of the third. This is visible in the same plots Fig. 2 at small values of  $d$ . The slope of the data points deviates from linearity and reduces in magnitude. Therefore, the fourth-order term is responsible for reducing the overall tidal force involving the leading and sub-leading term, consistent with the velocity independent 1PN correction to the Newtonian tidal force (see [55] and references therein):

$$\|\mathbf{F}_{1PN}\| \sim \frac{M_{td}^2 M_{tf}}{d^3} . \quad (17)$$

One feature of the model in Eq. (9) is that there are three velocity independent terms at the fourth-order in

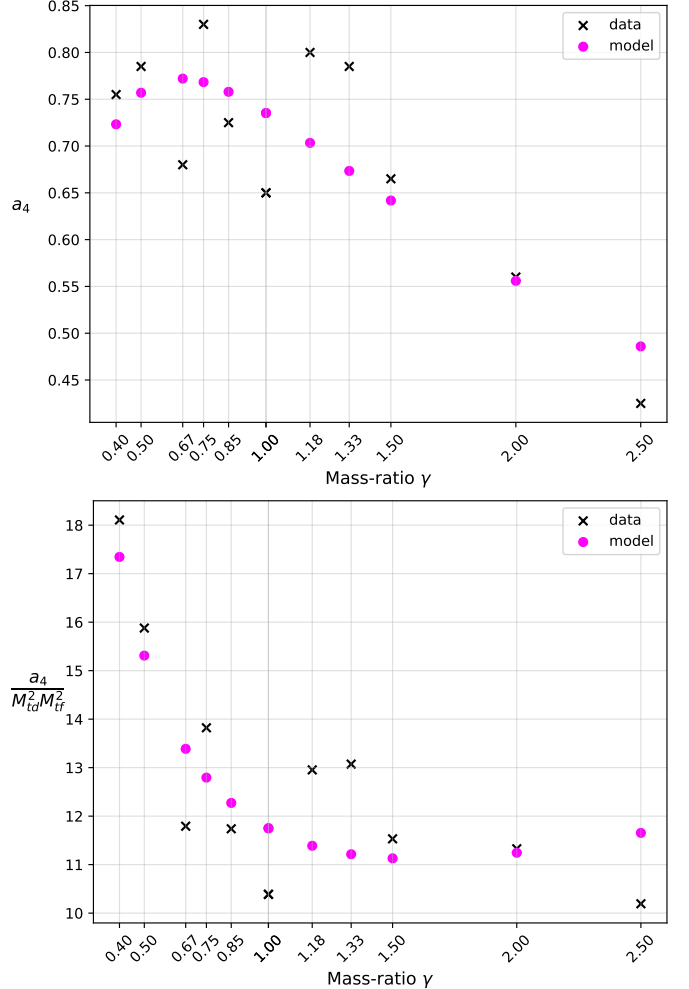


FIG. 4: The re-fit of  $a_4$  to the model of Eq. (9), with three terms, for the simulations  $q \geq 0.4$  (Model B). **Top:**  $a_4$  vs  $\gamma$ . **Bottom:**  $\frac{a_4}{M_{td}^2 M_{tf}^2}$  vs  $\gamma$ , i.e., the  $y$  axis of the bottom figure is obtained by scaling that in the top one by the mass factor  $M_{td}^2 M_{tf}^2$ . The data points are individual best fit parameters of Model B in Eq. (9) for both black holes in each simulation. The data points for the fit are in **black (crosses)** and the best fit model values are in **magenta (dots)**.

distance whereas there seems to be one term in the expression for the 1PN correction to the Newtonian gravitational force. It was verified that all three terms were necessary to explain the data points, which have a quadratic dependence on the mass-ratio  $q$  – as can be seen in the bottom panel of Fig. 4, and obtain a good fit to the data. This needs to be probed further in the future.

Finally, there is room for some error at the fourth-order in  $d$ . At this 1PN order, terms involving the relative velocities of the black holes would enter into the expansion of Eq. (7). These terms might be more contributing to the fourth-order term as the mass ratio decreases.

Therefore in order to analyze the multipole moment

data to infer the tidal coefficients at further smaller ratios than  $q = 0.4$ , one may need to take into account new terms involving velocities in the perturbative multipole expansion.

To further check the precision of these fits, we considered multiple sets of data having various combinations of our simulations, with additional configurations for intermediate  $q = \{0.6, 0.7\}$ ; excluding a few configurations randomly; or even adding/removing a few lower  $q \leq 0.6$ . Across these sets, we find  $\alpha_{12}$  to be  $\approx -1.0$  and  $\alpha_{21} \approx -5.3$ . Based on the results, we conclude that the tidal Love numbers at the leading order ( $\alpha_{12}$  and  $\alpha_{21}$ ) are estimated at a higher precision than for those at the sub-leading order ( $\alpha_{13}$ ,  $\alpha_{22}$  and  $\alpha_{31}$ ). This is reasonable since we are attempting to estimate the coefficients of the sub-leading order terms, to which there are three contributions (Eq. (9)). The contribution of the fourth-order term is not visible until the late inspiral phases of the evolution – i.e., at smaller values of  $d$  (as can be seen in Fig. 2). It has the largest impact during this phase, where the number of data points is significantly less to estimate it more precisely. The estimates for the tidal Love numbers at the fourth order may be expected to be computed with more accuracy by increasing the number of simulations.

## VI. DISCUSSION AND CONCLUSIONS

The primary goal of this paper was to study the tidal effects on horizons during the inspiral phase of binary black hole mergers. Past studies have examined tidal perturbations of isolated black holes, but this is the first time that tidal effects have been explored for a binary system using full numerical relativity simulations to deduce a black hole's tidal coefficients.

We used source multipoles computed on the marginally outer trapped surfaces for this analysis. We simulated non-spinning BBH with varying mass ratios  $q \in [0.4, 1]$ . The tidal coefficients defined here are a convenient way of quantifying the tidal deformability of black holes in a binary system. This approach does not involve the field multipole moments that are defined far away from the system, nor do they involve assuming a matter distribution whose compactness limit is taken to describe the black hole case. They are computed on space-like dynamical horizons. Also, these numbers are dimensionless and should be independent of the system considered i.e. same for all black holes (of any mass and spins) in General Relativity. We computed five tidal Love numbers which characterize the  $l = 2$  mass multipolar deformations of the dynamical horizon geometry at the leading and sub-leading order: two at the leading order and three at the sub-leading order.

The relations in Eqs. (7), (8) and (9), together with the best-fit parameters listed in Table II, show how the mass multipole moment of the horizon evolves in relation to the dynamics of the system in a binary black hole

merger scenario, apart from describing the evolution of tidal deformations. We find that the evolution of the multipole moments can be described quite accurately by the model in Eq. (7) up to the merger.

Here, it must be noted that for simulations of lower mass-ratios we notice an increase in the error of our fits to numerical data, which can be attributed to the increasing importance of the terms involving relative velocities of the black holes. In principle, more tidal Love numbers at successively higher orders can be computed in the manner described here given that the numerical simulations are carried out at sufficiently high resolution. It will be important to examine those cases with higher resolution runs in the future.

Analogous to the treatment of neutron star tidal deformability, a source-independent definition of the tidal deformation of black hole horizon using the source/geometric multipole moments of the horizon must also be possible. This would involve studying the perturbation of the geometry of an otherwise isolated horizon due to the external perturbing fields, and finding a relation between them – a quest that may be pursued in a future work.

## ACKNOWLEDGMENTS

This research was supported in part by a grant from the Navajbai Ratan Tata Trust. V.P is funded by Shyama Prasad Mukherjee Fellowship, (CSIR). The numerical simulations for this paper were performed on the Perseus and Pegasus clusters at The Inter-University Centre for Astronomy and Astrophysics, Pune, India (IUCAA).

## Appendix A: Distance measure

An estimate of the distance between the two black holes is required to calculate the tidal coefficient  $\alpha_{21}^{(2)}$ . We now discuss various choices for this distance measure and describe how we compute it from the numerical simulations. In the simulations we carried out, the numerical evolution uses a coordinate system described in [56]. We define and compute the following measures of distances of separation between the black holes:

- The Euclidean distance between the geometric centroids of the individual apparent horizons of the two black holes.
- Newtonian proper distance.
- Post-Newtonian (PN) distances up to second-order (PN1, PN2).

We explain each of these definitions below.

## 1. Euclidean distance

We use the coordinate locations of the geometric centroids  $((x_1, y_1, z_1)$  and  $(x_2, y_2, z_2)$ ) of the individual horizons of the two black holes to define a simple Euclidean distance measure. The distance is then defined by:

$$d = \sqrt{(x_1 - x_2)^2 + (y_1 - y_2)^2 + (z_1 - z_2)^2}. \quad (\text{A1})$$

### a. Newtonian proper distance

Kepler's third law for orbiting binaries can be used to calculate the distance of separation between the center of masses of the orbiting objects:

$$T^2 = kd^3. \quad (\text{A2})$$

We compute the instantaneous time period of the quasi-circular configuration by using the instantaneous frequency of the gravitational waves emitted from the system. We use the extracted gravitational radiation at  $100M$  from the center of the system for this purpose.

### b. Post-Newtonian distances

Using a method similar to the one described above for computing the Newtonian proper distance, we can compute proper distances to any Post Newtonian order by using an appropriate PN corrected version of Kepler's third law. Using this method, we compute PN1 and PN2 distances between the centers of the black holes.

### c. Choosing the distance measure

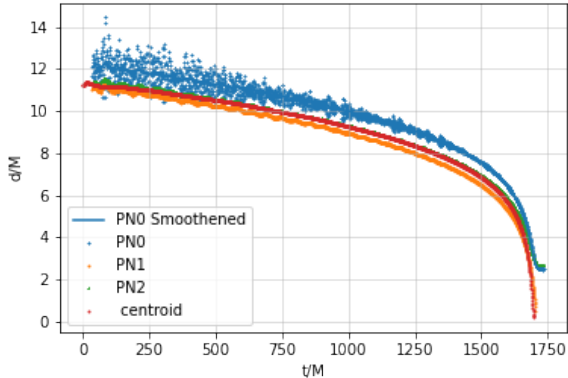


FIG. 5: The various distance measures for the  $q = 0.4$  simulation.

The plot for these distance measures for one of our simulations is shown in Fig. 5 for illustration.

It is observed that although the simple Euclidean distance measure seems less appropriate in comparison with the rest of the proper distance measures, it is the closest to the second-order Post-Newtonian distance measure. For any given simulation, the maximum cumulative (RMS) deviation between the simple Euclidean and other distance measures was found to be less than few times the initial separation. Further, the cumulative deviation with the PN2 distance measure was found to be the least for the simple Euclidean distance measure. Therefore, throughout the analysis, we choose to work with this distance measure.

The simple Euclidean distance measure also closely matches the Newtonian evolution of the separation between the two black holes. This can be found by means of simple fitting [57].

---

[1] R. A. Brooker and T. W. Olle, “Apsidal-motion constants for polytropic models,” *MNRAS* **115**, 101 (1955).

[2] Eanna E. Flanagan and Tanja Hinderer, “Constraining neutron star tidal Love numbers with gravitational wave detectors,” *Phys. Rev. D* **77**, 021502 (2008), arXiv:0709.1915 [astro-ph].

[3] Thibault Damour and Alessandro Nagar, “Relativistic tidal properties of neutron stars,” *Phys. Rev. D* **80**, 084035 (2009), arXiv:0906.0096 [gr-qc].

[4] James M. Lattimer and Madappa Prakash, “The Equation of State of Hot, Dense Matter and Neutron Stars,” *Phys. Rept.* **621**, 127–164 (2016), arXiv:1512.07820 [astro-ph.SR].

[5] B. P. Abbott *et al.* (LIGO Scientific, Virgo), “GW170817: Measurements of neutron star radii and equation of state,” *Phys. Rev. Lett.* **121**, 161101 (2018), arXiv:1805.11581 [gr-qc].

[6] Soumi De, Daniel Finstad, James M. Lattimer, Duncan A. Brown, Edo Berger, and Christopher M. Biwer, “Tidal Deformabilities and Radii of Neutron Stars from the Observation of GW170817,” *Phys. Rev. Lett.* **121**, 091102 (2018), [Erratum: *Phys. Rev. Lett.* 121, 259902 (2018)], arXiv:1804.08583 [astro-ph.HE].

[7] Collin D. Capano, Ingo Tews, Stephanie M. Brown, Ben Margalit, Soumi De, Sumit Kumar, Duncan A. Brown, Badri Krishnan, and Sanjay Reddy, “Stringent constraints on neutron-star radii from multimessenger observations and nuclear theory,” *Nature Astron.* **4**, 625–632 (2020), arXiv:1908.10352 [astro-ph.HE].

[8] Philippe Landry and Eric Poisson, “Relativistic theory of surficial love numbers,” *Phys. Rev. D* **89**, 124011 (2014).

[9] Thibault Damour and Orchidea Maria Lecian, “On the gravitational polarizability of black holes,” *Phys. Rev. D* **80**, 044017 (2009), arXiv:0906.3003 [gr-qc].

[10] Taylor Binnington and Eric Poisson, “Relativistic theory of tidal love numbers,” *Phys. Rev. D* **80**, 084018 (2009).

[11] Paolo Pani, Leonardo Gualtieri, Andrea Maselli, and Valeria Ferrari, “Tidal deformations of a spinning compact object,” *Phys. Rev. D* **92**, 024010 (2015), arXiv:1503.07365 [gr-qc].

[12] Alexandre Le Tiec, Marc Casals, and Edgardo Franzin, “Tidal Love Numbers of Kerr Black Holes,” (2020), arXiv:2010.15795 [gr-qc].

[13] Alexandre Le Tiec and Marc Casals, “Spinning Black Holes Fall in Love,” (2020), arXiv:2007.00214 [gr-qc].

[14] Thibault Damour and Alessandro Nagar, “Relativistic tidal properties of neutron stars,” *Phys. Rev. D* **80**, 084035 (2009).

[15] Abhay Ashtekar and Badri Krishnan, “Isolated and dynamical horizons and their applications,” *Living Rev. Rel.* **7**, 10 (2004), arXiv:gr-qc/0407042.

[16] Ivan Booth, “Black hole boundaries,” *Can. J. Phys.* **83**, 1073–1099 (2005), arXiv:gr-qc/0508107.

[17] Sean A. Hayward, “Black holes: New horizons,” in *Recent developments in theoretical and experimental general relativity, gravitation and relativistic field theories. Proceedings, 9th Marcel Grossmann Meeting, MG’9, Rome, Italy, July 2–8, 2000. Pts. A–C* (2000) pp. 568–580, arXiv:gr-qc/0008071 [gr-qc].

[18] Eric Gourgoulhon and Jose Luis Jaramillo, “A 3+1 perspective on null hypersurfaces and isolated horizons,” *Phys. Rept.* **423**, 159–294 (2006), arXiv:gr-qc/0503113.

[19] Matt Visser, “Black holes in general relativity,” PoS **BHSGRANDSTRINGS2008**, 001 (2008), arXiv:0901.4365 [gr-qc].

[20] Jose Luis Jaramillo, “An introduction to local Black Hole horizons in the 3+1 approach to General Relativity,” *Int. J. Mod. Phys. D* **20**, 2169 (2011), arXiv:1108.2408 [gr-qc].

[21] Valerio Faraoni and Angus Prain, “Understanding dynamical black hole apparent horizons,” *Lecture Notes in Physics* **907**, 1–199 (2015), arXiv:1511.07775 [gr-qc].

[22] Roger Penrose, “Gravitational collapse and space-time singularities,” *Phys. Rev. Lett.* **14**, 57–59 (1965).

[23] Daniel Pook-Kolb, Ofek Birnholtz, José Luis Jaramillo, Badri Krishnan, and Erik Schnetter, “Horizons in a binary black hole merger I: Geometry and area increase,” (2020), arXiv:2006.03939 [gr-qc].

[24] Daniel Pook-Kolb, Ofek Birnholtz, José Luis Jaramillo, Badri Krishnan, and Erik Schnetter, “Horizons in a binary black hole merger II: Fluxes, multipole moments and stability,” (2020), arXiv:2006.03940 [gr-qc].

[25] Lars Andersson, Marc Mars, Jan Metzger, and Walter Simon, “The Time evolution of marginally trapped surfaces,” *Class. Quant. Grav.* **26**, 085018 (2009), arXiv:0811.4721 [gr-qc].

[26] Lars Andersson, Marc Mars, and Walter Simon, “Stability of marginally outer trapped surfaces and existence of marginally outer trapped tubes,” *Adv. Theor. Math. Phys.* **12** (2008), arXiv:0704.2889 [gr-qc].

[27] Daniel Pook-Kolb, Ofek Birnholtz, Badri Krishnan, and Erik Schnetter, “Self-intersecting marginally outer trapped surfaces,” *Phys. Rev. D* **100**, 084044 (2019).

[28] Daniel Pook-Kolb, Ofek Birnholtz, Badri Krishnan, and Erik Schnetter, “Interior of a binary black hole merger,” *Phys. Rev. Lett.* **123**, 171102 (2019).

[29] Daniel Pook-Kolb, Robie A. Hennigar, and Ivan Booth, “A Pair of Pants for the Apparent Horizon,” (2021), arXiv:2104.10265 [gr-qc].

[30] Ivan Booth, Robie A. Hennigar, and Daniel Pook-Kolb, “Ultimate fate of apparent horizons during a binary black hole merger I: Locating and understanding axisymmetric marginally outer trapped surfaces,” (2021), arXiv:2104.11343 [gr-qc].

[31] Abhay Ashtekar, Jonathan Engle, Tomasz Pawłowski, and Chris Van Den Broeck, “Multipole moments of isolated horizons,” *Class. Quant. Grav.* **21**, 2549–2570 (2004), arXiv:gr-qc/0401114.

[32] Erik Schnetter, Badri Krishnan, and Florian Beyer, “Introduction to dynamical horizons in numerical relativity,” *Phys. Rev. D* **74**, 024028 (2006), arXiv:gr-qc/0604015.

[33] Luciano Rezzolla, Rodrigo P. Macedo, and Jose Luis Jaramillo, “Understanding the ‘anti-kick’ in the merger of binary black holes,” *Phys. Rev. Lett.* **104**, 221101 (2010), arXiv:1003.0873 [gr-qc].

[34] Miriam Cabero and Badri Krishnan, “Tidal deformations of spinning black holes in Bowen-York initial data,” *Class. Quant. Grav.* **32**, 045009 (2015), arXiv:1407.7656 [gr-qc].

[35] Norman Gürlebeck, “No-hair theorem for Black Holes in Astrophysical Environments,” *Phys. Rev. Lett.* **114**, 151102 (2015), arXiv:1503.03240 [gr-qc].

[36] Abhay Ashtekar, Miguel Campiglia, and Samir Shah, “Dynamical Black Holes: Approach to the Final State,” *Phys. Rev.* **D88**, 064045 (2013), arXiv:1306.5697 [gr-qc].

[37] Steven Brandt and Bernd Brügmann, “A simple construction of initial data for multiple black holes,” *Phys. Rev. Lett.* **78**, 3606–3609 (1997).

[38] John G. Baker, Manuela Campanelli, C. O. Lousto, and R. Takahashi, “Modeling gravitational radiation from coalescing binary black holes,” *Phys. Rev.* **D65**, 124012 (2002), arXiv:astro-ph/0202469 [astro-ph].

[39] Olaf Dreyer, Badri Krishnan, Deirdre Shoemaker, and Erik Schnetter, “Introduction to Isolated Horizons in Numerical Relativity,” *Phys. Rev.* **D67**, 024018 (2003), arXiv:gr-qc/0206008.

[40] Frank Löffler, Joshua Faber, Eloisa Bentivegna, Tanja Bode, Peter Diener, Roland Haas, Ian Hinder, Bruno C. Mundim, Christian D. Ott, Erik Schnetter, Gabrielle Allen, Manuela Campanelli, and Pablo Laguna, “The Einstein Toolkit: A Community Computational Infrastructure for Relativistic Astrophysics,” *Class. Quantum Grav.* **29**, 115001 (2012), arXiv:1111.3344 [gr-qc].

[41] EinsteinToolkit, “Einstein Toolkit: Open software for relativistic astrophysics,” <http://einstein toolkit.org/>.

[42] Marcus Ansorg, Bernd Brügmann, and Wolfgang Tichy, “A single-domain spectral method for black hole puncture data,” *Phys. Rev. D* **70**, 064011 (2004), arXiv:gr-qc/0404056.

[43] Miguel Alcubierre, Gabrielle Allen, Bernd Brügmann, Thomas Drumlitsch, Jose A. Font, Philippos Papadopoulos, Edward Seidel, Nikolaos Stergioulas, Wai-Mo Suen, and Ryoji Takahashi, “Towards a stable numerical evolution of strongly gravitating systems in general relativity: The Conformal treatments,” *Phys. Rev.* **D62**, 044034 (2000), arXiv:gr-qc/0003071 [gr-qc].

[44] Miguel Alcubierre, Bernd Brügmann, Peter Diener, Michael Koppitz, Denis Pollney, Edward Seidel, and Ryoji Takahashi, “Gauge conditions for long term numerical black hole evolutions without excision,” *Phys. Rev.* **D67**, 084023 (2003), arXiv:gr-qc/0206072 [gr-qc].

[45] J. David Brown, Peter Diener, Olivier Sarbach, Erik Schnetter, and Manuel Tiglio, “Turduckening black holes: an analytical and computational study,” *Phys. Rev. D* **79**, 044023 (2009), arXiv:0809.3533 [gr-qc].

[46] Denis Pollney, Christian Reisswig, Erik Schnetter, Nils Dorband, and Peter Diener, “High accuracy binary black hole simulations with an extended wave zone,” *Phys. Rev. D* **83**, 044045 (2011).

[47] Jonathan Thornburg, “Finding apparent horizons in numerical relativity,” *Phys. Rev. D* **54**, 4899–4918 (1996), arXiv:gr-qc/9508014.

[48] Jonathan Thornburg, “A Fast Apparent-Horizon Finder for 3-Dimensional Cartesian Grids in Numerical Relativity,” *Class. Quant. Grav.* **21**, 743–766 (2004), arXiv:gr-qc/0306056.

[49] Barry Wardell, Ian Hinder, and Eloisa Bentivegna, “Simulation of GW150914 binary black hole merger using the Einstein Toolkit,” (2016), <https://doi.org/10.5281/zenodo.155394>.

[50] James Healy, Carlos O. Lousto, and Yosef Zlochower, “Remnant mass, spin, and recoil from spin aligned black-hole binaries,” *Phys. Rev. D* **90**, 104004 (2014), arXiv:1406.7295 [gr-qc].

[51] James Healy and Carlos O. Lousto, “Remnant of binary black-hole mergers: New simulations and peak luminosity studies,” *Phys. Rev. D* **95**, 024037 (2017).

[52] RITcatalog, “RIT Catalog for Numerical Simulations,” <https://ccrg.rit.edu/~RITCatalog/>.

[53] Vaishak Prasad, “A movie showing the deformation of horizon geometry of horizons in a binary black hole merger.” [https://drive.google.com/file/d/1HDKOEHD8LC09CW--mvq12MaT0vV5\\_cvg/view?usp=sharing](https://drive.google.com/file/d/1HDKOEHD8LC09CW--mvq12MaT0vV5_cvg/view?usp=sharing) (2021).

[54] Hank Childs, Eric Brugger, Brad Whitlock, Jeremy Meredith, Sean Ahern, David Pugmire, Kathleen Biagas, Mark Miller, Cyrus Harrison, Gunther H. Weber, Hari Krishnan, Thomas Fogal, Allen Sanderson, Christoph Garth, E. Wes Bethel, David Camp, Oliver Rübel, Marc Durant, Jean M. Favre, and Paul Navrátil, “Visit: An end-user tool for visualizing and analyzing very large data,” in *High Performance Visualization—Enabling Extreme-Scale Scientific Insight* (2012) pp. 357–372.

[55] Peng Xu and Ho Jung Paik, “First-order post-newtonian analysis of the relativistic tidal effects for satellite gradiometry and the mashhoon-theiss anomaly,” *Phys. Rev. D* **93**, 044057 (2016).

[56] Jonathan Thornburg, “A fast apparent horizon finder for three-dimensional cartesian grids in numerical relativity,” *Classical and Quantum Gravity* **21**, 743–766 (2003).

[57] Nicholas Choustikov, “The einstein toolkit: A student’s guide,” (2020), arXiv:2011.13314 [gr-qc].